



LUND
UNIVERSITY

Summarising Constraints On Dark Matter At The Large Hadron Collider

Isabelle John

Thesis submitted for the degree of Bachelor of Science
Project Duration: Sep – Dec 2016, half-time
Supervised by Caterina Doglioni

Department of Physics
Division of Particle Physics
December 2016

Abstract

Dark matter is estimated to make up around 25% of the Universe [1], but it is not known what dark matter is. In particle physics, mediators of dark matter are used to model interactions of dark matter particles with known particles (Standard Model particles). These mediator particles can be produced from two quarks or gluons in high-energetic proton-proton collisions, and decay immediately back into Standard Model particles – or into dark matter particles.

We simulated different scenarios to study the signal shape of this mediator particle. The event generation was done by using MadGraph 5. We used samples with the mediator only decaying into quarks to compare them to samples in which the mediator can additionally decay into dark matter, as well as various other changes to investigate the different shapes of the mediator signal.

Abbreviations

BBN	Big Bang nucleosynthesis
CMB	cosmic microwave background
DM	dark matter
FWHM	full width half maximum
LHC	Large Hadron Collider
LO	lowest-order
MACHO	massive compact halo object
MC	Monte Carlo
MOND	modified Newtonian dynamics
NLO	next-to-leading order
QCD	quantum chromodynamics
RMS	root mean square
SM	Standard Model
SUSY	supersymmetry
WIMP	weakly interacting massive particle

Acknowledgements

Thanks very much to Caterina, my supervisor, for teaching and explaining me everything, and for all the help throughout the project work and writing. I learnt a lot, and I appreciate it very much.

Contents

1	Introduction	1
1.1	Evidence for dark matter	1
1.2	Explanations for dark matter	2
1.3	The Standard Model and beyond	3
1.3.1	Dark matter particles	5
1.4	Experiments and searches for dark matter	7
1.4.1	Direct detection	7
1.4.2	Indirect detection	8
1.4.3	Collider experiments	8
2	Theoretical and experimental details of this work	10
2.1	The mediator Z'	10
2.2	Summarising constraints on dark matter	11
2.2.1	Explanation of the features of the summary plot	12
2.3	Programs and simulations	14
2.4	13 TeV dijet generation	14
2.4.1	Samples	14
2.4.2	Data processing	15
3	Results	17
3.1	Cross sections	17
3.2	Experimental and theoretical widths	17
4	Discussion	22
4.1	Cross sections	22
4.2	Comparison of experimental and theoretical widths	23
4.3	Conclusion	24
5	Outlook	25
	Bibliography	26
	Appendices	28
	Appendix A Crystal Ball Function	29
	Appendix B Fits	30
	Appendix C Superimpositions	32

Chapter 1

Introduction

There are many things we do not understand yet in our Universe, and one of them is dark matter. It makes up about 83% of the total matter, and about 25% of the total constituents of the Universe. Only 5% of the Universe is the visible matter that we know. The remaining 70% of the energy budget of the Universe is dark energy [1].

Being one of the biggest mysteries in our Universe, there are different approaches that scientists have adopted to theorise and discover dark matter.

Dark matter could be a new type of particle that has never been observed. This coincides with indications that the Standard Model of particle physics – a theory of all known particles and their interactions – itself is not complete either, and could be extended with particles such as dark matter. If dark matter particles exist and interact with these Standard Model particles, these interactions can be observed. The interactions can take place through a mediator particle that can be created in high-energetic proton-proton collisions at collider experiments such as the Large Hadron Collider (LHC), when quarks and gluons interact. Being short-lived, this mediator will decay quickly, producing collimated beams of hadrons (jets) that can be measured and used to trace back to the properties of the mediator particle.

With so little known about dark matter, searches are important, and so are their interpretation in terms of dark matter theories. An important ingredient of this interpretation is the simulation of dark matter mediator decays. In this thesis, we simulated the creation and decay of these mediator particles into two jets.

Firstly, a theoretical background is given about dark matter and the Standard Model, and methods to detect dark matter. Then the model on which this thesis is based is explained, and how simulations can be used to determine constraints on dark matter particles. After that, the different samples that are simulated are described, and the results analysed and discussed. Lastly, a brief outlook on future work is given.

1.1 Evidence for dark matter

In the 1930s, Fritz Zwicky observed the Coma cluster, a large cluster of galaxies, and tried to determine its total mass with different methods. The mass could either be determined by measuring the absolute luminosity as an approximation of the total mass in the cluster, or inferred from the internal rotation of the cluster where the cluster is approximated to behave like a solid.

The different methods did not give coinciding results. Instead, it seemed like that there was more matter than was visible to explain the velocity dispersion of the individual galaxies in the cluster. Since this missing matter did not seem to radiate any light, it was called “dark matter” as opposed to the light-emitting luminous matter that stars are made of [1, 2].

It took until the 1970s until more attention was paid to this problem when Vera Rubin and others found further evidence for dark matter within galaxies by looking at their rotational velocities [3].

Most of the luminous mass is concentrated in the central bulge of a galaxy, with the

amount of luminous mass decreasing towards the outer parts of the galaxy. If the galaxy has a mass M , and a star with mass m orbits the galaxy in the outer regions with a distance r from the centre, the gravitational force F experienced by the star is

$$F = \frac{GMm}{r^2} = \frac{mv^2}{r}.$$

It follows that the rotational velocity v of the star is $v = (GM/r)^{1/2}$, which means that the velocity of the star is expected to decrease with $r^{-1/2}$. However, observations show that the velocity does not decrease, but instead stays roughly constant with increasing distance from the centre. This leads to the conclusion that the amount of mass within a certain distance from the centre must be proportional to the distance. Since the amount of luminous matter decreases, there must be some non-luminous matter that accounts for the discrepancy in mass in the outer regions of a galaxy – dark matter [1].

More evidence for dark matter was found with gravitational lensing.

From General Relativity it is known that, due to their gravity, massive objects (e.g. galaxies or clusters of galaxies) are able to bend light that passes them closely, similar to a lens bending light. A source object (e.g. a star or a galaxy) behind the lens appears distorted, since its light is bent when it passes close enough to the lensing object to be affected by the gravity. If the source is far away from the lens or not well-aligned, the lensed object just appears distorted, as not all parts of the source are lensed in the same way. This is called weak gravitational lensing. In strong gravitational lensing, the source is perfectly aligned behind the lens so that the image of the source appears as a ring, often called Einstein-ring [4].

Similarly, dark matter can act as gravitational lenses, with the difference that it is an invisible lens. Thus, from both weak and strong lensing, the amount and distribution of dark matter in a certain region can be inferred by looking at the distortion of galaxies and clusters of galaxies [4].

1.2 Explanations for dark matter

There are many theories to explain the cosmological observations of missing matter. Some examples of these theories of what dark matter could be are given here.

- **MOND** Since dark matter shows attractive gravitational properties and does not seem to interact with matter in any other way, it could simply be that gravity itself is not fully understood. Newton's description of gravity could be incomplete, and gravity could behave differently on larger scales. The most common alternative gravity theory is MOND (Modified Newtonian Dynamics).

MOND proposes that Newton's Second Law, $F = ma$, is in fact $F = \mu(a)ma$ where $\mu(a) = a/a_0$. a_0 is a constant for gravity so that $\mu(a)$ approaches 1 on smaller scales, but has a significant effect on larger scales such as galaxies. Good results are obtained for $a_0 \approx 1.2 \times 10^{-10} \text{ m/s}^2$ [1]. The previously mentioned flat rotation curves of galaxies can then be explained, as the gravitational force with MOND becomes

$$F = \frac{GMm}{r^2} = ma\mu(a) \Rightarrow a = \frac{\sqrt{GMa_0}}{r},$$

giving the centripetal acceleration

$$\frac{\sqrt{GMa_0}}{r} = \frac{v^2}{r} \Rightarrow v = (GMa_0)^{1/4}$$

which is constant, and thus gives a constant rotational velocities for galaxies, as is consistent with observations.

Even though MOND can explain problems on galactic scales, it cannot account for the larger structures in the Universe [1]. Even combined with another alternative theory, the tensor-vector-scalar (TeVeS) that explains additional relativistic phenomena, alternative gravity cannot fully account for dark matter [4].

- **MACHOs** Not all matter in the Universe is so luminous that it can be easily observed. There are faint stars such as brown dwarfs whose matter is not taken into account when mass calculations are based on just the luminous matter. There is also a large amount of gas in galaxies that is not necessarily luminous, but provides mass as well. Some of the missing matter could therefore just be ordinary matter with very low luminosities. Some of this matter could also be part in very massive dark objects in the halo of a galaxy. These objects are called massive compact halo objects (MACHOs) and can be black holes or even planets and asteroids, or primordial black holes that formed shortly after the Big Bang in regions of high density [1, 4].

But even considering the various types of faint, ordinary matter, all this is still not enough to explain all of the effects that dark matter shows [4].

- **Particles** Dark matter could be a new type of matter and consist of particles that have not yet been discovered, going beyond the currently known particles. In fact, measurements suggest that only around 17% of the Universe is made up of luminous matter, with the remaining matter being dark matter [1]. These particles as an explanation for dark matter is what this thesis concentrates on.

1.3 The Standard Model and beyond

In particle physics, the Standard Model is a theory that tries to explain the known particles and their properties and interactions. An overview of the constituents of the Standard Model is given in figure 1.1.

There are six fundamental leptons and six fundamental quarks, each group with three different generations of which the lowest generation is a stable particle. The leptons consist of electron, muon and tauon, and three corresponding neutrinos, electron neutrino, muon neutrino and tau neutrino.

The quarks come in up (u) and down (d) quark, charm (c) and strange (s) quark, and bottom (b) and top (t) quark, with the top quark being the heaviest and the up quark being the lightest.

Leptons and quarks are spin-1/2 particles, called fermions. There are also integer-spin particles, called bosons. These gauge bosons carry the forces between the fundamental particles during particle interactions.

The gauge bosons of the weak interaction are W^\pm and Z^0 . Electromagnetic interaction takes place via photon (γ) exchange. The strong interaction takes place via gluon (g)

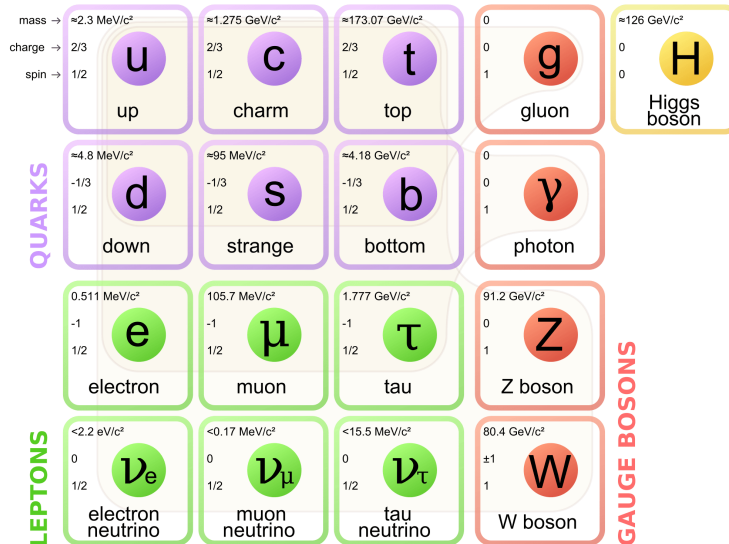


Figure 1.1: The Standard Model of elementary particles [6]

exchange. Particles gain their masses by interactions with the Higgs particle (H), a spin-0 boson.

These particles, including the anti-particles of the leptons and quarks (particles with exactly the same properties, except for opposite electrical charge), build the Standard Model.

Composite particles made up of quarks are called hadrons. These can either be mesons that consist of a quark and an anti-quark, or baryons that are made up of three quarks, like the proton or neutron (uud and udd, respectively), or three anti-quarks (anti-baryon). Since most of the visible matter is made up of protons and neutrons, it is also referred to as baryonic matter. The quarks are held together in hadrons by the strong force.

However, there are unsolved issues that the Standard Model does not explain, leading to searches and theories extending beyond the Standard Model to possibly find missing particles, some of which could be dark matter particle candidates.

One of these extensions of the Standard Model is supersymmetry (SUSY). Each fermion (spin-half particle) has a super-partner with spin-0, and each boson (integer-spin) has a spin-half super-partner. Stable supersymmetric particles are possible weakly interacting massive particle (WIMP) candidates and thus also candidates for dark matter [5]. This means that dark matter could be part of a more general theory such as SUSY.

Jets

A jet of particles is produced when a gluon or quark is fragmented in a high-energy collision.

Quarks and gluons – collectively also called partons – possess a colour charge, and interact with each other via the strong interaction. This is described by quantum chromodynamics (QCD). Colour-charged particles cannot exist unbound, which means that quarks and gluons are confined to baryons or mesons where all the colour charges add up to a neutral charge. If high-energetic quarks or gluons are produced in a particle collision, they immediately decay to build other particles with neutral colour charge. This process is called hadronisation and results in the creation of many particles, that in turn, depending on their energy, can decay further and produce more hadrons until low-energetic stable

particles are created. Therefore, in detection images, quarks and gluons are always seen as jets. A single jet is produced by a single quark or gluon, two jets from two (possibly a quark-antiquark pair), and so on [5, 11].

Jet searches can, for example, be used to find dark matter candidates in high-energetic particle collisions. Particles that immediately decay after their production can be indirectly discovered with jet searches because they are visible as an excess around their mass, referred to as a resonance.

1.3.1 Dark matter particles

Relic density

Particles were created during the Big Bang. The Universe was extremely dense and hot and dominated by quark-gluon plasma, with matter and radiation being in thermal equilibrium. Therefore, the Universe was opaque to light. Only a short time after that, when the Universe further expanded and cooled, it was possible for the quarks and gluons to combine to hadrons and create protons. Since the Universe was still hot and dense, the nucleosynthesis of light elements and their isotopes was possible, creating nuclei such as hydrogen, deuterium, helium and lithium. This process is called Big Bang nucleosynthesis (BBN), and it is the earliest epoch in the history of the Universe from which data is obtainable. Thus, from the pre-BBN era, no data is available, which is presumably the time when most dark matter was formed together with Standard Model particles. The particles observed today are relics from this early era [1, 8].

Around 380 000 years after the Big Bang, the Universe reached a temperature of around 3000 K and was cool enough for protons and electrons to form atoms. This process is known as recombination. As more and more atoms were formed, the travelling distances of the photons increased because they were less scattered or absorbed by other particles. At some point, the photons were able to decouple from the matter and travel freely, and the Universe became transparent to radiation. These first photons are still detectable as the cosmic microwave background (CMB). Since they have been travelling through the expanding Universe for around 13.7 billion years, their original high-energetic, short wavelength was extremely redshifted into the microwave regime ($z = 1100$). This corresponds to a temperature of 2.73 K [8].

The CMB can be used to determine the amount of dark matter and the other constituents¹ of the Universe:

The Universe contains matter (m), radiation (r) and vacuum (Λ). The energy density Ω of the Universe is then given by

$$\Omega = \frac{\rho_m}{\rho_c} + \frac{\rho_r}{\rho_c} + \frac{\rho_\Lambda}{\rho_c} = \Omega_m + \Omega_r + \Omega_\Lambda.$$

Looking at the cosmic microwave background, ripples are visible. These fluctuations are of the order of 10^{-5} and come from temperature differences due to inhomogeneities in the early Universe – early evidence for the now-observable large scale structure in the Universe. Fitting the angular power spectrum of the CMB with the above mentioned

¹The contents of the Universe determine its future. This depends on the value of the critical density ρ_c . If the total density of the Universe is smaller than the critical density, $\rho_{total} < \rho_c$, then the expansion of the Universe is decelerated until it reaches a turning point after which the Universe starts collapsing. If $\rho_{total} > \rho_c$, the Universe keeps expanding.

energy densities, the abundance of the components of the Universe are roughly estimated to be $\Omega_m = 0.30$ (0.25 dark matter and 0.05 baryonic matter), $\Omega_r = 5 \times 10^{-5}$ and $\Omega_\Lambda = 0.70$.² The most recent measurements of the CMB were made by the Planck satellite in 2013 [4, 8, 9].

These values show that the Universe is dominated by vacuum energy of which nothing is known, except that it seems to cause the expansion of the Universe to be accelerated. It is therefore referred to as dark energy.

The Universe contains dark energy (70%), dark matter (25%), baryonic matter (5%) and a negligibly small amount of radiation [9]. The standard model of cosmology tries to explain these occurrences. Since most of the dark matter contents are required to be non-relativistic (cold), and the Universe is dominated by vacuum energy, the model is referred to as Λ CDM [4].

Other properties of dark matter

Besides having gravitationally attractive properties, dark matter does not seem to interact in any other way. There is no evidence that it interacts with light in any way, which is one reason why it has not been discovered yet. Its electromagnetic coupling must therefore be very small or its mass very heavy so that electromagnetic interactions have almost no consequences.

Since dark matter is still present today, it must be either stable or have a lifetime longer than the current age of the Universe.

Most of the dark matter has to be dissipationless, meaning that the dark matter cannot cool down by radiating photons as baryonic matter does. This is why it does not cool down and collapse into the centre of a galaxy, but instead stays in the halo³ [1, 4].

Dark matter seems to be mostly collisionless. Evidence for this can be found in the Bullet cluster where two clusters of galaxies collide and pass through each other. The galaxies are barely affected by the collision, and their behaviour can be described by a collisionless fluid. The gas between the galaxies (mainly hydrogen gas) is collisional, which slows the gas down so that it is stripped away from the galaxies. Looking at weak gravitational lensing effects, one would expect the peak of the lensing to be strongest where most of the visible matter – the gas – is if there were alternative gravity. This is not the case, instead the strongest gravitational lensing effects are observed where the galaxies are. MOND cannot explain this observation, but collisionless dark matter can. The dark matter contents of the two clusters must still be near the galaxies and since the galaxies have passed through each other collisionless it is indicated that dark matter also behaves mostly collisionless [1, 4].

Hot dark matter is relativistic, warm dark matter just on the verge of not being relativistic, and cold dark matter non-relativistic. Simulations suggest that most of the dark matter should be cold or warm, but not hot, meaning that dark matter moves non-relativistically [4].

There are several candidates for dark matter particles, for example axions, sterile neutrinos and WIMPs.

Axions are very light particles, and are a candidate for cold dark matter. They are bosons that result from spontaneous symmetry breaking. There could be other axion-like

²Since this approximately adds up to 1, this means that the curvature of the Universe is flat.

³However, there are theories that part of the dark matter could be dissipative and form a “dark disk”, similar to the way baryonic matter forms disk-like galaxies. The dissipation could be done via “dark photons” [1].

particles resulting from other broken symmetries [1].

Sterile neutrinos are a result of neutrino mass oscillations. But instead of interacting via the weak force, as the neutrinos in the Standard Model do, sterile neutrinos only interact gravitationally, and are therefore a dark-matter candidate [1].

WIMPs are Weakly Interacting Massive Particles and include for example supersymmetric partners of the Standard Model particles. They are the dark matter candidates relevant in this thesis.

1.4 Experiments and searches for dark matter

There are many searches that try to find dark matter. Figure 1.2 shows what kind of interactions the different experiments are based on. The detection of dark matter can be done using several methods; by direct and indirect detections, or by creating WIMPs as dark matter particle candidates in collider experiments. The latter is what this thesis concentrates on; simulations of WIMP interactions that could be mediated by particles.

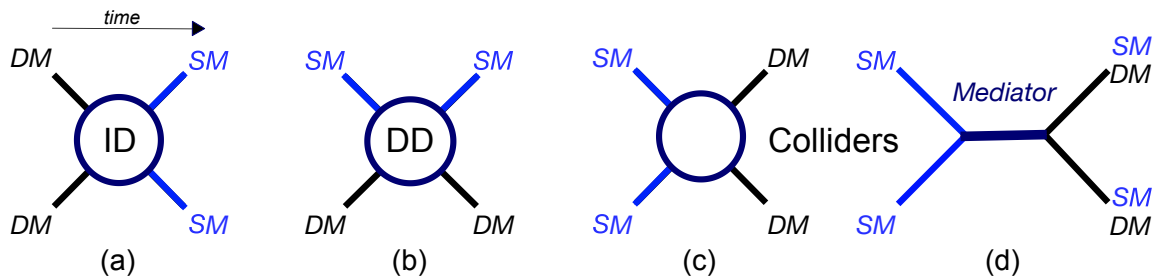


Figure 1.2: Overview of the different interactions of dark matter with Standard Model particles. (a) represents indirect detection where two DM particles produce SM particles and (b) represents direct detection where a DM particle interacts with a SM particle. The interaction in collider experiments are shown in (c) and (d) where two SM particles become DM particles (c), or become a mediator that can decay to DM as well as SM (d). The circles indicate that the type of interaction is not known. Sketch by Caterina Doglioni.

1.4.1 Direct detection

Experiments such as XENON or CDMS [7] try to detect the interaction of a dark matter particle passing through Earth with a Standard Model particle, see figure 1.2 (b). Since these interactions are weak and rare, the detectors are very large and, to minimise background signals as much as possible, are built underground to be shielded from cosmic rays and radioactivity [1].

Alternatively, direct detection experiments can be small and sensitive, like the CRESST experiment that uses superconductors that are cooled down to very low temperatures. Dark matter particles would be detected when interacting with the detector material, causing it to heat up [7].

1.4.2 Indirect detection

When satellites and telescopes scan the sky, they sometimes find signals with unknown origin. Some of them could indicate the presence of dark matter, annihilating or decaying into Standard Model particles, and producing the observed signals, see figure 1.2 (a). For example, the production of a pair of photons, $\chi\chi \rightarrow \gamma\gamma$, or a photon and a Z boson, $\chi\chi \rightarrow \gamma Z$, would result in a monochromatic signal, i.e. a signal of a specific wavelength. However, none of the observed signals are yet confirmed to originate from dark matter interactions.

Another example for such an observation is the 511 keV signal detected by the satellite INTEGRAL. It is a signal originating from the galactic centre and created by electron-positron annihilation. The positron source could be from dark matter particles, that annihilate into electron-positron pairs, or a dark matter particle decaying into a lighter dark matter particle and an electron-positron pair [1].

Neutrino detectors could also be used to detect signs of dark matter from the Sun. As dark matter is mostly present in the halo of the galaxy, and Sun and Earth move through parts of the halo, it is possible that dark matter particles – WIMPs in this case – scatter with the baryonic matter of the Sun or Earth. They can lose so much energy that they become gravitationally bound, and eventually annihilate with other WIMPs, producing Standard Model particles. Since neutrinos are only weakly interacting, they are the only decay products that can easily escape from the Sun or Earth and can then be detected by detectors such as IceCube. These neutrinos would have much higher energies than other neutrinos (e.g. the neutrinos produced in the Sun) and thus could be recognised as the decay products of dark matter WIMPs [1].

1.4.3 Collider experiments

In collider experiments, two Standard Model particles are accelerated to high energies and collided with each other, with the aim to produce dark matter particles, see figure 1.2 (c) and (d). This thesis looks at proton-proton collisions as carried out at the Large Hadron Collider (LHC).

Detectors and the ATLAS experiment

The ATLAS detector is part of the LHC at CERN, and used for researching for example the fundamental forces or theories beyond the Standard Model such as dark matter and supersymmetry [10].

Particle detectors are built of several layers around the particle beam where the collisions happen. The innermost layer is a tracking chamber that is able to track any electromagnetically charged particles such as electrons or protons. Around this is the electromagnetic calorimeter where electromagnetically interacting particles interact with matter and start showering, i.e. creating a cascade of more particles when interacting with the detector material. After this follows the hadron calorimeter where strongly-interacting particles are detected by creating hadronic showers. The outer layer is the muon chamber to track muons which do not interact otherwise.

Due to their weak interaction, dark matter particles cannot be tracked in these kinds of detectors, but their production can be inferred from the detection of the Standard Model particles produced in the same collision.

Since transverse momentum – the momentum component perpendicular to the direction of the beam – must be conserved, the total transverse momentum in the initial and final state of the collision has to be zero. Missing transverse momentum (also called \cancel{E}_T or E_T^{miss}) can occur if invisible particles decay and recoil against visible Standard Model particles.

If WIMPs are produced, they pass through the detector unnoticed, but a large amount of missing transverse momentum can indicate the WIMPs, and it is possible to infer the mass of the WIMP [12].

In this thesis, the mediator of dark matter interactions with Standard Model particles is produced by the collision of two Standard Model particles, and decays both to dark matter particles and Standard Model particles, see figure 1.2 (d).

Chapter 2

Theoretical and experimental details of this work

This section explains the model used for the studies in this thesis, in which a mediator particle decays to quarks. It also describes dark matter searches in proton-proton collision experiments and how these can be used to constrain the properties of dark matter. Furthermore, details about the implementation of the simulations and the handling of the generated data are given.

2.1 The mediator Z'

In this model, the interaction between dark matter and Standard Model particles takes place via a mediator Z' . At the LHC, two proton beams are collided with each other at energies high enough that the quarks of one proton interact with the quarks of another proton. Therefore, the collision of the protons can be simplified to the collision of two quarks.

The two quarks in the initial state of the interaction collide and annihilate to form an unknown and unstable mediator Z' that immediately decays into a pair of stable or long-lived dark matter particles, or back into two quarks. Hence, the mediator has two different final states that it can decay into.

Assuming that dark matter similarly to Standard Model particles decays into two particles (possibly a particle and an antiparticle) of equal mass and energy, dark matter decays only occur if the mass of the mediator is at least double the mass of one dark matter particle, i.e. $m_{Z'} \geq 2m_{DM}$.

If the mediator decays only into quarks, it is called off-shell, see figure 2.1. If the mediator can decay into dark matter particles, see figure 2.2, as well as quarks, it is called on-shell.

The strength of a particle being coupled to interact via a certain force is given by a coupling constant [11]. The couplings of the mediator to the quarks g_q and to dark matter g_{DM} can be either vector couplings or axial vector couplings¹. The difference in the couplings lies in the parity. Vector couplings have negative parity and axial couplings have positive parity [11].

The mediator is leptophobic, meaning that no decays into leptons are possible; so the final state of the interaction excludes leptons.

The mediator has spin 1 and neutral charge, similar to the Standard Model Z boson of the weak interaction, and is supposedly massive [13].

The interaction of particles can be described by Feynman diagrams. In a so-called “s-channel” process, two particles annihilate into a mediator that subsequently decays again into two particles. The Feynman diagrams in figures 2.1 and 2.2 only show the lowest-order term (LO), but in reality there are more interactions possible; in the case of quarks and gluons, additional quarks and gluons are added to LO due to QCD processes. The lowest of these higher order terms is called next-to-leading order term (NLO) [5, 11].

¹In this thesis also shortened to “axial coupling”.

The mediator decays immediately after its production which means that it cannot be directly detected. It can only be seen as a resonance in the dijet final state, i.e. looking at the invariant mass of the dijet, there is a peak around the mass of the mediator. From the decay products of the mediator, it is possible to infer the properties of the mediator [1, 5].

In this model, the produced dark matter particles are WIMPs. This is the reason why they are not detectable in the detectors used in collision experiments.

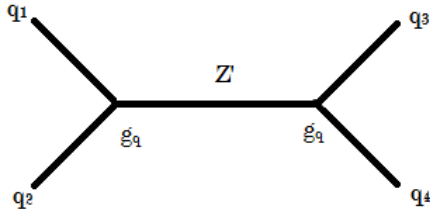


Figure 2.1: Feynman diagram for an off-shell mediator with coupling constants

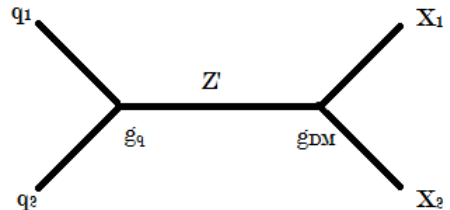


Figure 2.2: Feynman diagram for an on-shell mediator with coupling constants

2.2 Summarising constraints on dark matter

Even though no dark matter particle candidates have been observed yet, it is possible to constrain their properties, for example by using experimental data, theoretical models or simulations. This is the general aim: constraining dark matter energies with the knowledge we already have to guide experiments that search for dark matter particles. Since so little is known about dark matter, having directions on where to perform searches is important.

Figure 2.3 shows a summary of these constraints. The plot is created by plotting the mass of the dark matter m_{DM} against the mass of the mediator $m_{Z'}$ for a range of masses.

The results are obtained by comparing the theoretical cross sections to experimental cross sections that are obtained from simulating different samples. The cross section of an interaction is a measure of the probability for this interaction to occur. This means for example that the interaction probability is higher for higher cross sections [11].

To compare the theoretical and experimental cross sections, the following relation is used

$$\mu = \frac{\sigma_{exp}}{\sigma_{theo}}$$

where σ_{exp} and σ_{theo} are the observed and theoretical interaction cross sections, respectively. This is to determine whether a certain point can be excluded or not.

If $\mu > 1$, the experimental cross section is greater than the theoretical one, and so the experimental number of events is greater than the theoretically predicted number of events. Since this abundance could be caused by dark matter particles, or statistical fluctuations of the background, it is not possible to exclude this point.

If $\mu < 1$, the experimental cross section is smaller than the theoretical cross section. If dark matter had been there, the additional events would have been visible. Since this is not the case, the point can be excluded.

In these studies, the coupling constant between the mediator and dark matter particles was chosen to be $g_{DM} = 1$ and the coupling constant with quarks $g_q = 0.25$. Furthermore, the mediator Z' is an axial-vector mediator, meaning that both the couplings to dark matter as well as to Standard Model particles is an axial-vector coupling.

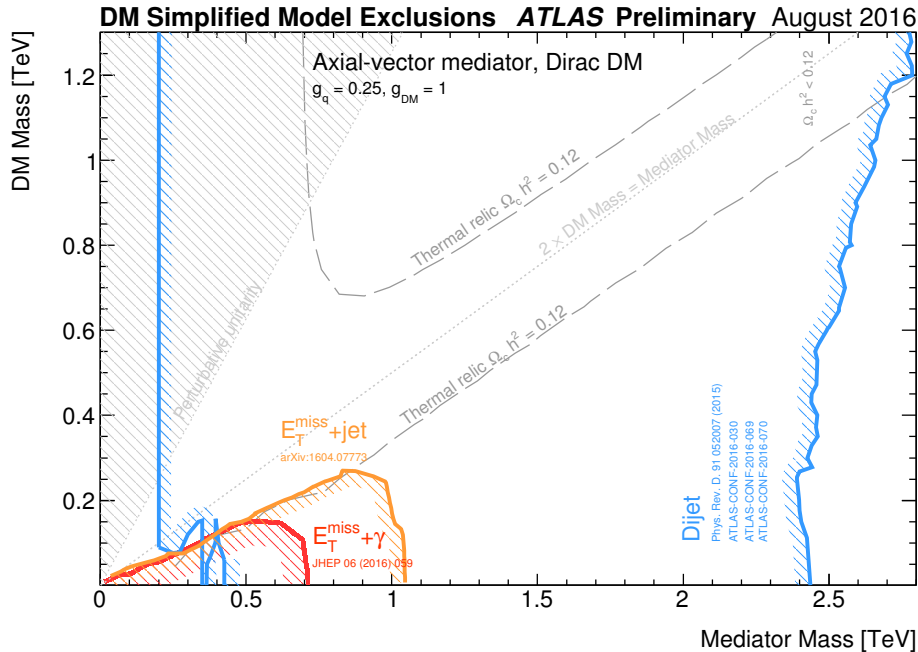


Figure 2.3: The dark matter summary plot, created by the ATLAS Dark Matter collaboration to summarise constraints on dark matter [14]

2.2.1 Explanation of the features of the summary plot

Perturbative unitarity

This region is excluded due to constraints of the model itself, i.e. the model is not theoretically valid in this region of the plot.

Thermal relic

Here the thermal relic density, i.e. the remnants of the dark matter particles produced during the Big Bang, is displayed. Only within this area, dark matter particle interaction through the mechanism described by this model is responsible for generating this relic density.

$\Omega_c h^2$ denotes the cold dark matter density of today. h is a parameter related to the Hubble constant H_0 , i.e. the ratio of the velocity of an object to its distance to us. h is given by $h = H_0 / (100 \text{ km}/(\text{s Mpc}))$. Current values of h are $h = 0.68$. For an energy density of dark matter $\Omega = 0.25$, this gives $\Omega_c h^2 = 0.12$ [8, 9].

Mono-X searches ($E_T^{miss} + X$)

Mono-X detections are collisions that result in, for example, a single photon – mono- γ – or similarly mono- W , mono- Z , but they can also result in monojets, i.e. a jet produced

from a single quark in the initial state. So far, the summary plot uses mono- γ 13 TeV and monojet 13 TeV searches to create exclusion regions. Figure 2.4 shows a Feynman diagram of mono-X processes.

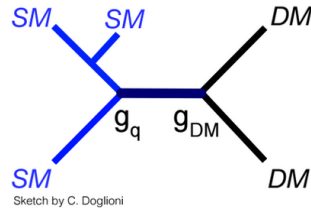


Figure 2.4: Feynman diagram representing the production of a mono-X in the initial state. Sketch by Caterina Doglioni.

Dijet searches

Dijets are produced from two quarks or gluons, see figures 2.1 and 2.2, or figure 1.2. Here, various dijet searches of different dijet-invariant masses and with different analyses are used to exclude large areas in the plot.

As can be seen, only a small area in the lower left part of the summary plot is left. This region satisfies cosmological constraints and is not (yet) experimentally excluded. To constrain the mass range that has to be searched for dark matter particle candidates as much as possible, the aim is to exclude as much as possible.

Another version of the summary plot is presented in figure 2.5. Here the coupling constants are $g_q = 0.1$ and $g_{DM} = 1.5$. In this plot, larger regions could not be excluded yet.

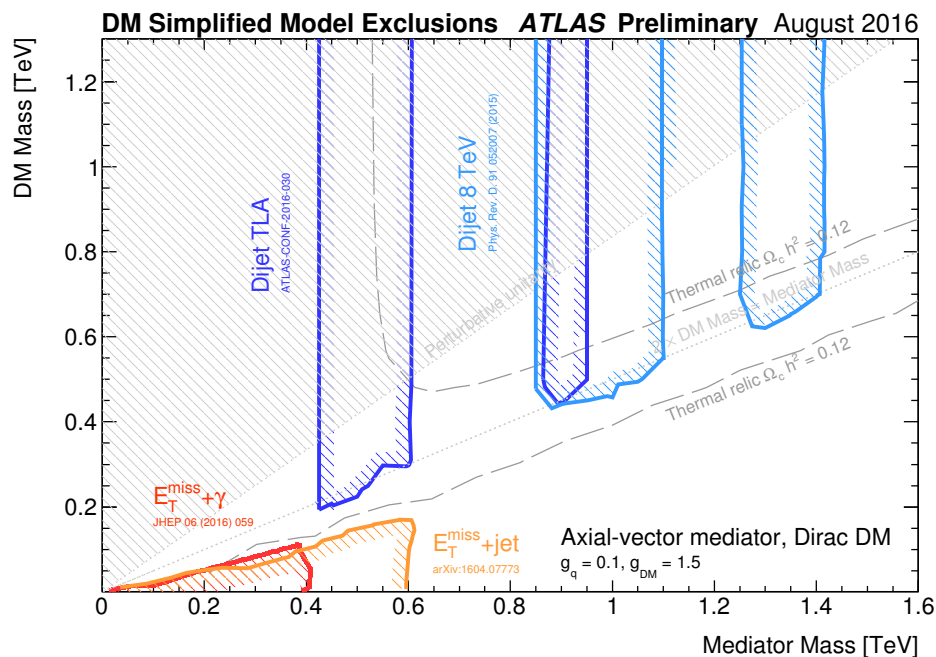


Figure 2.5: A variation of the above summary plot with coupling constants modified to $g_{DM} = 1.5$ and $g_q = 0.1$ [14]

It can be noted from the two summary plots that the exclusion regions depend on the coupling of the dark matter mediator with the Standard Model. This is a free parameter in this dark matter theory, and as such one has to be careful in interpreting these plots as full theories rather than example possibilities.

2.3 Programs and simulations

The events are generated by programs called Monte Carlo (MC) generators. These are useful to generate particle collision events, as they provide random numbers that are needed to create random collision events. Further randomness is also provided by for example the branching ratio (the probability of a certain decay) of the possible decays. They also encapsulate the physics processes in the collision.

To generate proton-proton collisions that produce the mediator Z' from two quarks in the initial state, and the mediator decay into two dark matter particles or again into two quarks, MadGraph 5 is used [15]. The simulation of the showering and hadronisation effects of the quarks in the final state creating the jets is done by using PYTHIA 8 [16].

The data is analysed using ROOT with Python (PyROOT) [17]. The code can be found on GitHub [18].

2.4 13 TeV dijet generation

In this work, we generated Z' decaying to dijet final states with centre-of-mass energy of 13 TeV with several extensions and changes to investigate the differences in the signal shape of the Z' resonance.

Following the summary plot, the coupling constants were $g_q = 0.25$ and $g_{DM} = 1$. If not otherwise stated, these were axial couplings. Similarly, only the leading-order term (LO) was generated; except in the cases where these features were added to test them, and in initial and final state all quarks except the top quark were used.

All generations were done for 20 000 events. The mass of the mediator Z' was always used as 2000 GeV, and the centre-of-mass energy of the dijet was always $\sqrt{s} = 13$ TeV.

2.4.1 Samples

In the following, the generated samples are described.

- Nominal sample: off-shell, axial: First we created a nominal sample to compare the other samples with changes to. In the simulation, the dark matter mass was set sufficiently high, so that only decays into quarks were possible. All couplings were axial couplings, with $g_{DM}^A = 1$ and $g_q^A = 0.25$.
- On-shell, axial: In a first comparison, we changed to an on-shell generation, where the mediator could decay into dark matter particles as well. The dark matter mass was $m_{DM} = 10$ GeV.
- Off-shell, vector: To see the different effects of vector and axial couplings, we generated an off-shell sample with vector couplings similar to the previously used axial couplings, i.e. $g_{DM}^V = 1$ and $g_q^V = 0.25$.

- On-shell, vector: We repeated the previous generation with an on-shell mediator and a dark matter mass of $m_{DM} = 10$ GeV as in the previous on-shell sample.
- Off-shell, axial, top: As the top quark was previously excluded in both initial and final state, we created a sample with top and anti-top quarks in both states.
- Off-shell, axial, QCD, NLO: In this generation, we allowed for QCD, hence adding the next-to-leading order term, and making the simulation more complex.

2.4.2 Data processing

For each sample, the experimental interaction cross section σ_{exp} was obtained from the output of the generation.

Furthermore, for each sample, the invariant mass of the dijet m_{jj} , the transverse momentum of the leading jet p_T , the pseudorapidity η and y^* were plotted. The rapidity y for each jet is given by

$$y = \frac{1}{2} \ln \left(\frac{E + p_z}{E - p_z} \right), \quad (2.1)$$

where E is the energy of the jet, and p_z is the momentum along the beam. The difference between the rapidities of two jets are invariant under boosts along the direction of the beam, i.e. they are the same in both frames. y^* is then given by

$$y^* = \frac{y_0 - y_1}{2}, \quad (2.2)$$

and is the mean value of the rapidity of the leading jet y_0 and the subleading jet y_1 , and therefore y^* is the rapidity for the two jets (the dijet) in the centre-of-mass frame [11, 19].

The pseudorapidity η , that can be used for negligible jet masses, is defined by

$$\eta = -\ln \left(\tan \frac{\theta}{2} \right) \quad (2.3)$$

where θ is the angle between the jet and the axis along the beam [11].

Since new physics events in dijet searches are usually produced centrally in the lab frame, as they are isotropic in the centre-of-mass frame, and to remove background, several cuts, as listed below, were applied to the generated data of all samples (m_{jj} , leading jet p_T , leading and subleading jet η , rapidity y^*).

- $|y^*| < 0.6$,
- leading jet $|\eta| < 2.8$,
- subleading jet $|\eta| < 2.8$,
- for transverse momentum: leading jet $p_T > 430$,

After applying the cuts, the peak of the m_{jj} distribution was fitted to obtain the width (the full width at half maximum – FWHM). The fit function used was the crystal ball function. It is similar to a Gaussian fit, but with more parameters which allows for a smoother fit, and makes the crystal ball function suitable for signal shapes like these. For more information on the crystal ball function, see appendix A and [20].

The peak of the distribution is the resonance of the mediator Z' ; therefore it is centred around the mass of the mediator, 2000 GeV. The range of the fit around this peak was chosen to be 2 times the root mean square (RMS) – for these samples usually around 900 to 1000 GeV – before and after the mass of the mediator to obtain a good fit. The RMS was obtained through an output of ROOT when plotting the distribution.

To determine whether a fit is good, we calculated the reduced χ^2 for each fit, i.e. χ^2/ndf where ndf is the number of degrees of freedom (the number of bins minus the number of parameters of the fit function). χ^2 is given by

$$\chi^2 = \sum_{n=1}^{n_{bins}} \left(\frac{f_i - y_i}{\sigma_i} \right)^2 \quad (2.4)$$

where y_i is the number of counts in the corresponding bin, f_i the corresponding value of the fit function, and σ_i the uncertainty of that value [13].

A value of the reduced χ^2 close to 1 indicates a good fit.

Theoretical widths

According to [12], the partial decay widths of the mediator Z' are separately calculated for decays into dark matter, $Z' \rightarrow \chi\tilde{\chi}$, and decays of the mediator into fermions, $Z' \rightarrow f\tilde{f}$, that is

$$\Gamma(Z' \rightarrow \chi\tilde{\chi}) = \frac{M_{Z'}}{12\pi} \sqrt{1 - 4z_\chi} \left[(g_\chi^V)^2 + (g_\chi^A)^2 + z_\chi \left(2(g_\chi^V)^2 - 4(g_\chi^A)^2 \right) \right] \quad (2.5)$$

and

$$\Gamma(Z' \rightarrow f\tilde{f}) = \frac{M_{Z'} N_c}{12\pi} \sqrt{1 - 4z_f} \left[(g_f^V)^2 + (g_f^A)^2 + z_f \left(2(g_f^V)^2 - 4(g_f^A)^2 \right) \right] \quad (2.6)$$

where $M_{Z'}$ is the mass of the mediator. g_χ^V and g_f^V are vector couplings, and g_χ^A and g_f^A are axial vector couplings. z_χ and z_f are given by $z_\chi = m_\chi^2/M_{Z'}^2$ and $z_f = m_f^2/M_{Z'}^2$, respectively, where m_χ and m_f are the masses of the dark matter particle and the fermion with $m_\chi = 10$ GeV and $m_f \approx m_{down} = 4.8 \times 10^{-3}$ GeV, respectively. For quarks, $N_c = 3$ and for leptons, $N_c = 1$.

However, the partial widths for fermions (in this case quarks) are only approximate, as this formula only enables the usage of one quark mass, whereas the generation is based on five or six quarks with different masses. It also only accounts for QCD effects at LO, not NLO.

If only decays into quarks are possible, then the partial width of the quarks is the total width of the signal. For the cases in which the mediator also decays into dark matter particles, the sum of the two partial widths gives the total width. The resonance width of the mediator broadens if the mediator is on-shell since the dark matter particles cannot be detected and therefore the uncertainty in the measurement increases [13].

Chapter 3

Results

This section presents the results of this study. It includes the cross sections obtained from the MC generators, the plots of relevant kinematic distributions from the generated events, the fit result and the values from the theoretical calculation for the width of the mediator. The results are used to investigate whether rescaling between the samples is possible or not.

3.1 Cross sections

An overview of the cross sections of all samples is given in table 3.1, including the uncertainties of the values. The unit of the cross section is picobarn (pb) where $1\text{b} = 10^{-24}\text{cm}^2$. Also given are the ratios of the cross sections of each sample with respect to the nominal sample, and the number of events for each sample that remained after applying the cuts.

Table 3.1: Experimental cross sections with errors and ratio to off-shell, axial sample, and the number of events that pass the cuts.

type	σ_{exp} [pb]	ratio	number of events after cuts
off-shell, axial	0.73027 ± 0.00063	1	9753
on-shell, axial	0.40269 ± 0.00038	0.551	9727
off-shell, vector	0.72523 ± 0.00063	0.993	9602
on-shell, vector	0.40119 ± 0.00044	0.549	9745
off-shell, axial, top	0.86645 ± 0.00071	1.312	9815
off-shell, axial, QCD, NLO	0.9634 ± 0.0053	1.186	8404

3.2 Experimental and theoretical widths

Figure 3.1 shows the number of events against the dijet invariant mass m_{jj} of the nominal sample (i.e. off-shell, axial coupling), including the fit. The peak is centred around 2000 GeV, the mass of the resonance Z' , with a long tail below that mass, but fewer entries above. It can be seen that the fit function does not cover the full height of the peak. The number of events at the peak is around 500 with the total number of events that remain after the cuts being 9753.

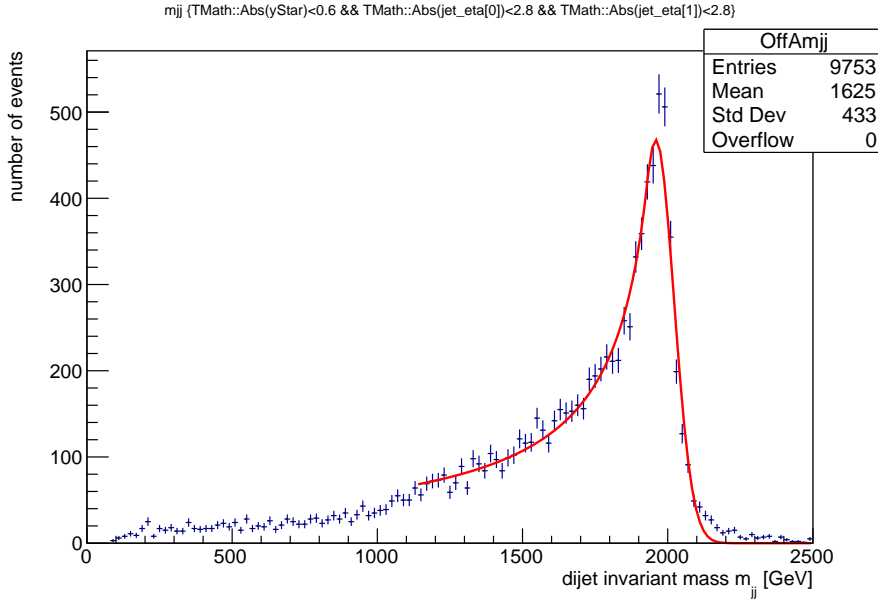


Figure 3.1: Dijet invariant mass of the nominal sample (off-shell, axial) with fitting curve.

Figures 3.2 and 3.3 display the fitted m_{jj} distributions in the on-shell, axial sample, and the sample including NLO, respectively. Plots for all other samples can be found in appendix B.

Figure 3.2 shows the m_{jj} distribution of the on-shell, axial coupling sample with a peak centred around the mass of the mediator. The fit was not able to cover the whole height of the peak. The number of events remaining after the cuts is 9727.

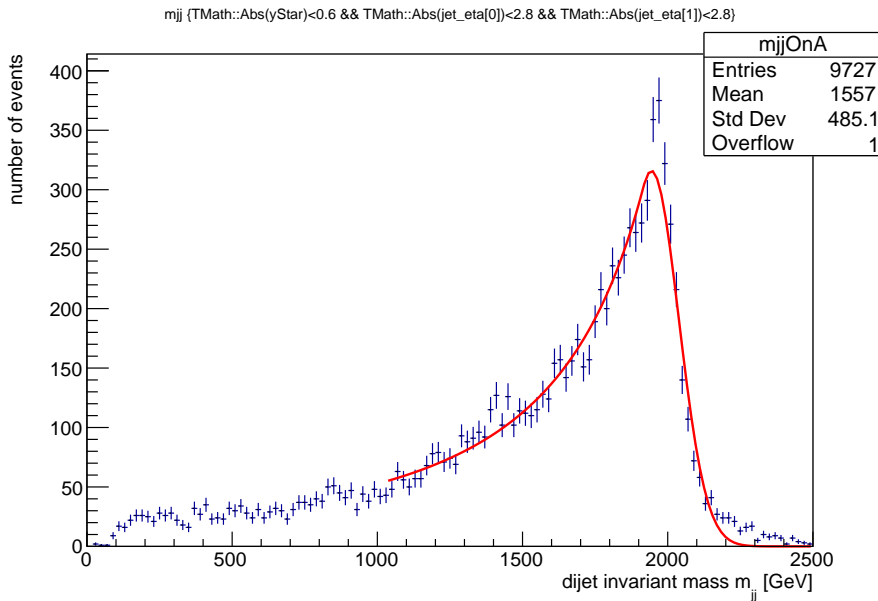


Figure 3.2: Fit of the m_{jj} distribution in the on-shell, axial sample

In figure 3.3, the m_{jj} distribution and fit of the off-shell, axial sample with NLO can be seen. The peak is centred around the mass of the resonance. In this case, the number of events remaining after the cuts is 8404.

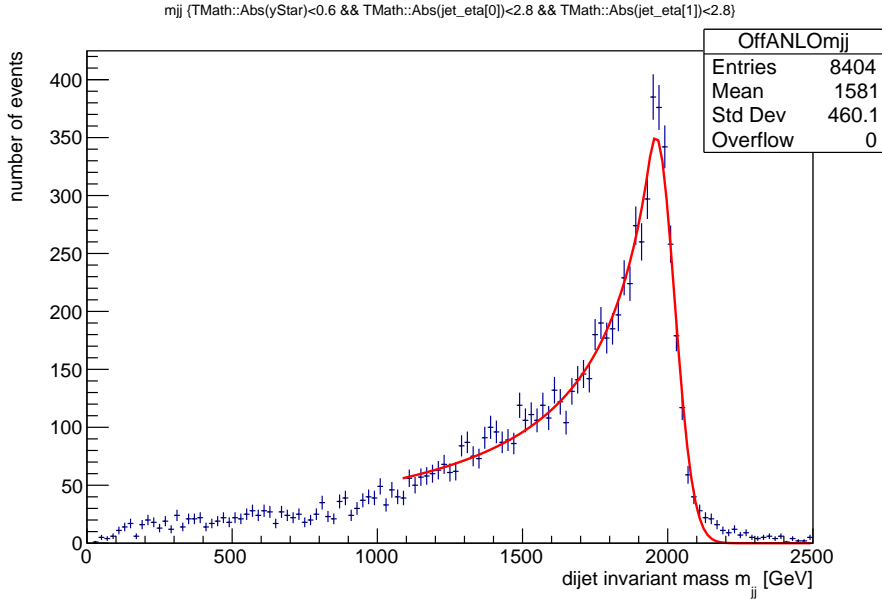


Figure 3.3: Fit of the m_{jj} distribution in the off-shell, axial, NLO sample

A summary of all the reduced χ^2 and experimental widths Γ_{exp} with uncertainties, obtained from the fits, is given in table 3.2.

Table 3.2: Reduced χ^2 of m_{jj} fit and experimental widths with errors, obtained from the simulations

type	reduced χ^2	Γ_{exp} [GeV]
off-shell, axial	4.1	62 ± 3
on-shell, axial	3.5	94 ± 4
off-shell, vector	4.6	59 ± 3
on-shell, vector	2.9	104 ± 4
off-shell, axial, top	3.8	63 ± 3
off-shell, axial, QCD, NLO	2.9	64 ± 3

Figures 3.4 to 3.6 show several overlaid m_{jj} distributions of different samples for comparison. More of these plots, such as a comparison of the vector coupling with off- and on-shell mediator, and overlaid plots of the leading jet p_T , η and y^* can be found in appendix C as well.

Figure 3.4 shows the comparison of on-shell and off-shell mediators, both with axial coupling. The sharper peak, printed in red, belongs to the off-shell sample, whereas the broader peak in blue represents the on-shell sample.

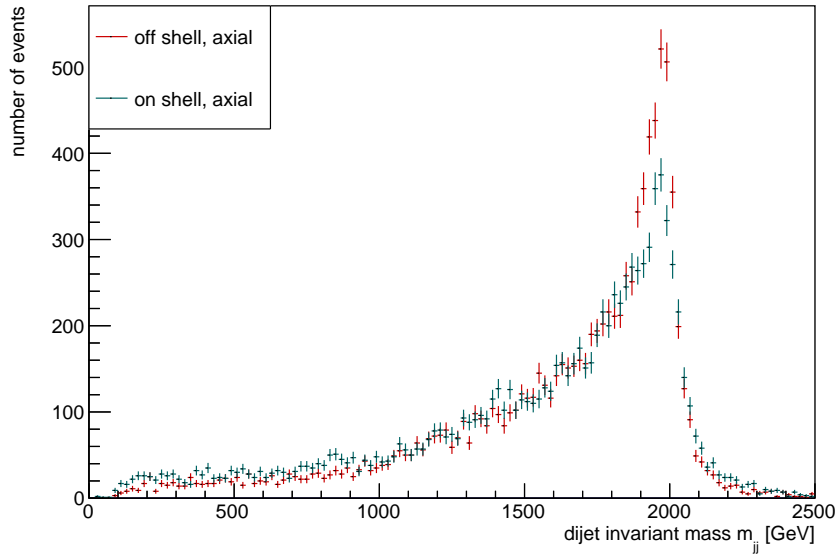


Figure 3.4: Comparison of m_{jj} between the nominal sample and the on-shell, axial sample

In figure 3.5 the nominal sample is compared to the sample that includes also the next-to-leading order term. The red points represent the LO sample, the blue points the NLO sample. It can be seen that the peak of the NLO sample is smaller than the peak of the LO sample, with fewer events remaining after the cuts.

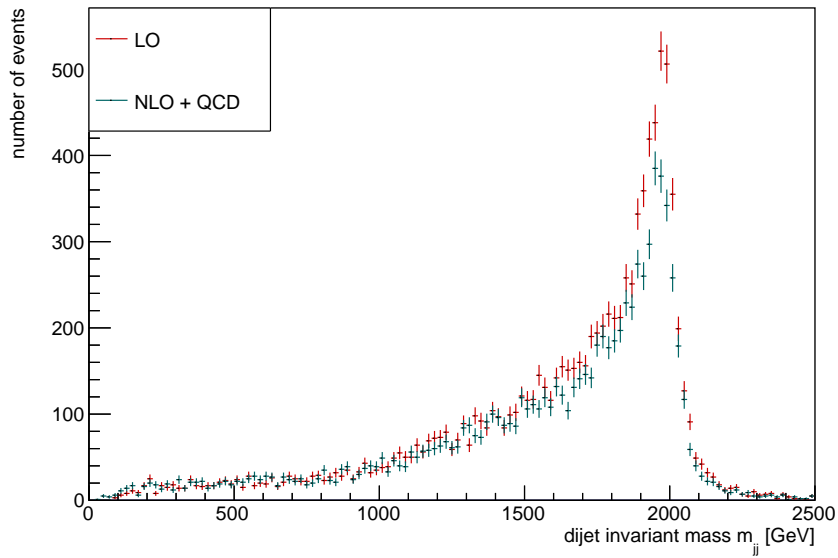


Figure 3.5: Comparison of m_{jj} between the nominal sample and the off-shell, axial sample including NLO.

Figure 3.6 shows two off-shell samples, one with axial coupling (red) and one with vector coupling (blue). Both curves possess a similar shape.

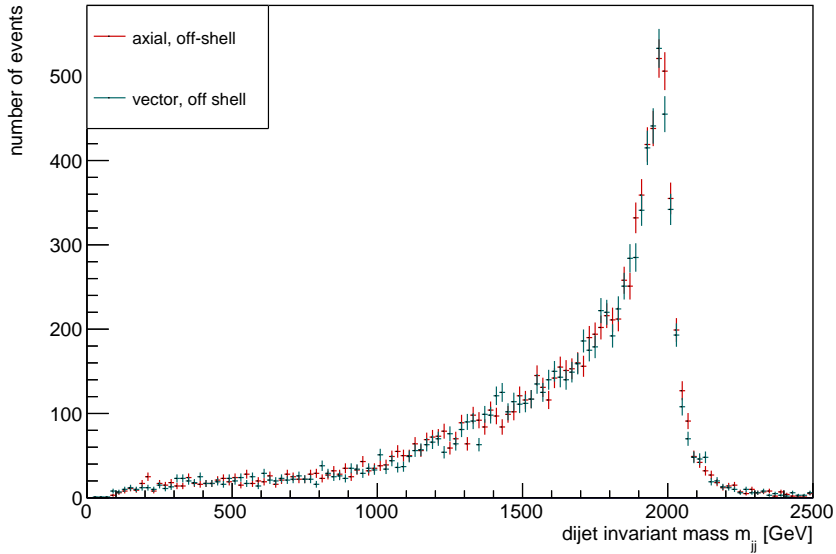


Figure 3.6: Comparison of m_{jj} between the nominal sample and the off-shell, vector sample.

Calculating the theoretical widths using equations 2.5 and 2.6, table 3.3 gives an overview of the theoretical and experimental widths of all simulations.

The calculation of the theoretical width for the sample including the top quark was not possible with equation 2.6, as this formula does not account for different quark masses. Neither could a theoretical width for the sample including NLO be calculated, as this computation is more complex.

Table 3.3: Comparison of the theoretical widths and experimental widths, obtained from the simulations

type	Γ_{theo} [GeV]	Γ_{exp} [GeV]
off-shell, axial	10	62 ± 3
on-shell, axial	63	94 ± 4
off-shell, vector	10	59 ± 3
on-shell, vector	63	104 ± 4
off-shell, axial, top	-	63 ± 3
off-shell, axial, QCD, NLO	-	64 ± 3

Chapter 4

Discussion

In this section, the results are analysed and discussed, comparisons are made between theoretical and experimental values, and differences are tried to be explained. Eventually, it is concluded what we can learn from the results of these simulations.

Firstly, it has to be determined if the differences between the various samples are significant. The difference between two results becomes significant if the two values are not within their errors.

An overview of comparisons of the cross sections and widths for the various samples with the nominal sample is given as follows:

- **axial vs vector:** In the off-shell case, the difference in the widths between axial and vector coupling are insignificant. The difference between the two widths becomes slightly larger in the on-shell samples compared to the off-shell samples.

The cross sections show a small difference; they are slightly smaller in the on-shell samples.

- **off-shell vs on-shell:** Changing from off-shell to on-shell coupling in both axial and vector coupling samples shows similar differences. In both cases, the width of the on-shell sample increases and the cross section decreases.
- **no top quark vs top quark:** When adding the top quark, the width remains similar, but the cross section increases.
- **LO vs NLO:** The width does not change when going from LO to NLO. However the NLO cross section is larger. Additionally it can be observed that the NLO sample has fewer number of events remaining after the cuts, as is shown in table 3.1.

4.1 Cross sections

The observed cross sections are given in table 3.1. These cross sections are the partial cross sections of decays into quarks. They are determined by multiplying the total cross section, that combines all possible interactions, with the branching ratio of the particular interaction of interest. The branching ratio is the fraction of the decays into a certain final state, in this case either quarks or dark matter particles. The given cross sections only display the fraction of decays into quarks, and not dark matter. In the off-shell samples, the total cross section equals the cross section of the quark interactions.

The cross sections are visually displayed in figure 4.1. It can be observed that the cross section increases compared to the nominal sample when adding the top quark¹ in initial and final state. This leads to a larger branching ratio which leads to an increased cross section.

Similarly, when adding NLO, previously suppressed interactions can take place now, increasing the branching ratio and therefore the cross section as well.

¹Since the top quark is very heavy and decays quickly, this also causes a higher abundance of b quarks and W bosons, the main decay products of the top quark [5].

However, when switching from off-shell samples to on-shell samples, the cross sections decrease. This is because in the on-shell sample the mediator can also decay into dark matter particles, so the cross section for decays into Standard Model particles is smaller than in the sample with only Standard Model particles. The branching ratio for decays into Standard Model particles is smaller since now also decays into dark matter particles are possible.

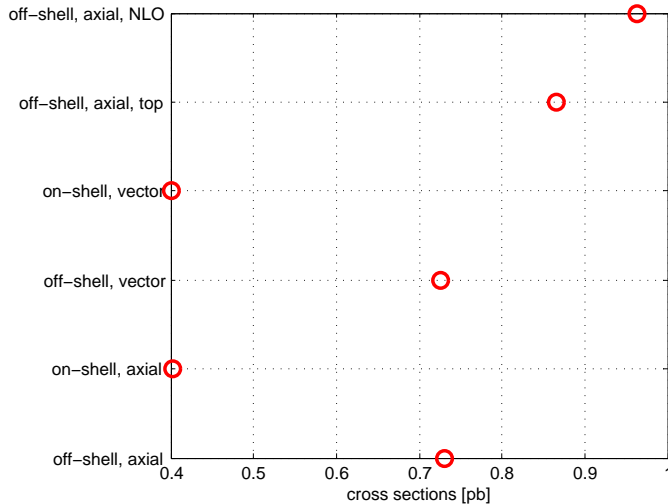


Figure 4.1: Overview of the experimental cross sections

4.2 Comparison of experimental and theoretical widths

The experimental widths can be seen in table 3.2 and figure 4.2 shows the experimental widths of all samples visually. The widths of all off-shell samples are similar; in fact the differences are within the errors, so they are insignificant. The width increases for the on-shell samples because if the mediator decays into dark matter particles, these escape the detector unnoticed, and the missing transverse energy leads to higher uncertainties around the resonance.

Comparing this to the theoretical widths displayed in table 3.3, it is noticeable that the theoretical and experimental widths greatly differ from each other. This is because the theoretical widths are determined before the parton shower, i.e. these widths are determined including the particles produced in the final state, but before the jet production. The experimental width is determined after that, so it also includes all the showering and jet production effects, and as more particles are involved, the uncertainty increases, which makes the widths significantly broader.

The larger theoretical widths for on-shell samples support the observation from the simulations. It can be noted that the ratio of the experimental widths between off-shell and on-shell is greater than the ratio of the theoretical widths; that is the experimental width in the on-shell sample is dominated by quarks, whereas the theoretical width in the on-shell sample is dominated by dark matter. This is explained considering that the experimental width is determined after the showering, and since dark matter does not interact in the detector, it does not add to the showering.

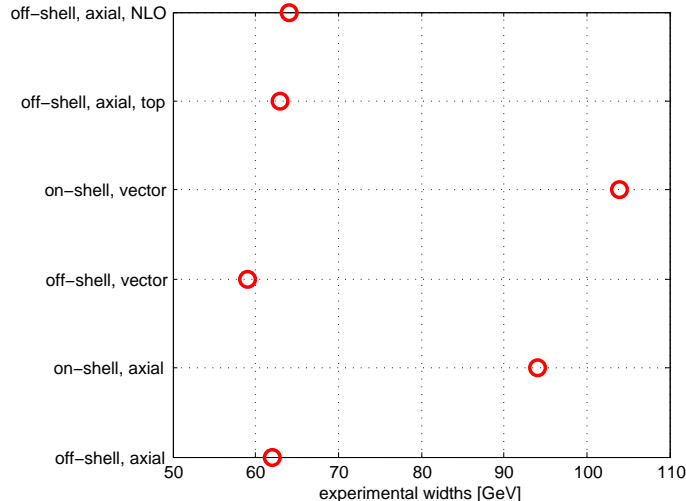


Figure 4.2: Overview of the experimental widths

4.3 Conclusion

The cross sections are given by the simulations. However, to determine the shape of the resonance signal, the generated data has to be further analysed and fitted to obtain the width of the distribution of the dijet invariant mass. It is convenient when different samples show a similar shape because that means that it is necessary to only determine the width of one sample, and use this to rescale to another sample, without having to generate both. The shape of the distribution is needed in later steps to determine over which region the integration of the signal has to be done when comparing it to the background.

Looking at the results of these simulations, several conclusions whether rescaling is possible and how it has to be done can be drawn.

There is no significant difference in the m_{jj} distribution widths for any off-shell samples, no matter if axial or vector coupling or with the additions of the top quark or NLO. The signal shape maintains a width equivalent to the other samples. This means that it is possible to rescale from the off-shell axial to any of the other off-shell samples, no matter if axial or vector coupling, or including top quarks or next-to-leading order terms. The ratio between the cross sections is used to rescale between the samples.

Going from LO to NLO is a special case, however. Since the shape to the nominal sample is the same, it is possible to rescale. To take care of the different cross sections, the ratio between the cross sections of LO and NLO is used; called the k -factor [21]. Additionally, it can also be observed that for all samples, except NLO, the number of events remaining after the cuts is similar. In the NLO sample the number of events is around 15% smaller, see table 3.1. Therefore, the difference in the number of events after the cuts has to be rescaled as well.

On the other hand, the width broadens clearly for both the on-shell mediator with vector and axial couplings compared to the off-shell counterparts. As the signal shape changes, rescaling from the nominal sample is not possible.

Chapter 5

Outlook

The aim of dark matter experiments is to discover particle evidence of dark matter that explains the cosmological observations. If so little is known about something that is sought for, constraining the dark matter properties even more and knowing what dark matter is not is crucial, and helps to set up new experiments, or to interpret the large amounts of data, and it also makes it possible to eliminate theoretical models by disproving them.

Searches from the LHC can be used for this purpose. The interpretation of these searches makes use of simulations of simplified models that have been studied in this thesis. Here, it has been shown that changing the parameters of these simulations does not require new, full event generations for these samples, but that one sample can be used to rescale to other similar samples with different parameters. This is an important finding for the interpretation of dark matter searches because it reduces the amount of computing power needed to generate these samples.

This thesis shows that simplified simulations can be used to rescale on larger samples. The models may be simplified but nonetheless we can learn from them. Understanding the simplified processes is the basis for understanding more complex processes and for extending models.

Further analysis of the simplified models of dark matter is needed to refine the values, and cover more possible scenarios. The simulations can be extended to even higher masses of mediator as well as dark matter particles, and they can be done for different coupling constants of the mediator. It was also assumed that there is one coupling constant for all quarks – in fact they could have individual constants; and the same is possible for different dark matter particles. Leptons have completely been omitted from these simulations and the summary plot, but there are other searches including them in final states such as the dilepton search [22].

However, it has to be kept in mind that these models and results are in the caveat of simplifications. In reality, the processes and interactions are likely much more complex, and could also include processes that we do not even know about yet.

Even though current experiments have not found dark matter candidates yet, the results help to constrain dark matter particles. The constraints can be used to create new and better experiments with focus on those energies where dark matter particles could be existent. However, it is not only the theoretical aspects that are able to refine models and predict more properties of dark matter, but also the technical advancements that make it possible to search at even higher energies that are likely required to produce and detect dark matter particles, or allow for even more sensitive detectors that can measure the smallest recoil energies of electrons or atoms after an interaction with a dark matter particle.

With improving experiments and the support of theories and simulations to set a frame for the experiments and guide the searches, it will only be a question of time when the first dark matter candidates are observed, if they indeed exist.

In the end, we hope that particle physics experiments will find evidence of new particles that complete the Standard Model, explain dark matter and maybe even require new theories.

Bibliography

- [1] Graciela B. Gelmini *TASI 2014 Lectures: The Hunt for Dark Matter*. 2015. arXiv: <https://arxiv.org/abs/1502.01320>
- [2] Fritz Zwicky *On The Masses of Nebulae and of Clusters of Nebulae*. Astrophysical Journal vol. 86, p.217, October 1937
- [3] Vera Rubin, W. Kent Ford, Jr *Rotation Of The Andromeda Nebula From A Spectroscopic Survey Of Emission Regions*. Astrophysical Journal, vol. 159, p.379, February 1970
- [4] Justin Read *Dark Matter*. 2016. url: <https://indico.lucas.lu.se/event/399/material/3/0?contribId=0>
- [5] B.R. Martin and G. Shaw *Particle Physics*. Third Edition. John Wiley & Sons Ltd; 2008
- [6] Figure of the Standard Model. url: https://commons.wikimedia.org/wiki/File:Standard_Model_of_Elementary_Particles.svg, accessed 15/12-2016
- [7] T. Undagoitia and L. Rauch *Dark matter direct-detection experiments*. September 2015. arXiv: <https://arxiv.org/pdf/1509.08767v1.pdf>
- [8] Andrew Liddle *An Introduction to Modern Cosmology*, Third edition, John Wiley & Sons Ltd; 2015
- [9] Planck Collaboration *Planck 2013 results. XVI. Cosmological parameters*. arXiv: <https://arxiv.org/pdf/1303.5076v3.pdf>
- [10] ATLAS. <http://atlas.cern>, accessed 22/11-2016
- [11] Mark Thomson *Modern Particle Physics*, Cambridge University Press, United Kingdom, 2016
- [12] M. Chala, F. Kahlhoefer, M. McCullough, G. Nardini, K. Schmidt-Hoberg *Constraining Dark Sectors with Monojets and Dijets*. June 2015. arXiv: <https://arxiv.org/abs/1503.05916>
- [13] M. Fairbairn, J. Heal, F. Kahlhoefer and P. Tunney *Constraints on Z' models from LHC dijet searches*. May 2016. arXiv: <https://arxiv.org/pdf/1605.07940v1.pdf>
- [14] ATLAS and CMS Collaborations *Summary plots for axial vector simplified DM models*. url: https://atlas.web.cern.ch/Atlas/GROUPS/PHYSICS/CombinedSummaryPlots/EXOTICS/index.html#ATLAS_DarkMatter_Summary, <https://cds.cern.ch/record/2208044>
- [15] J. Alwall, M. Herquet, F. Maltoni, O. Mattelaer, T. Stelzer *MadGraph 5: Going Beyond*. June 2011. arXiv: <https://arxiv.org/pdf/1106.0522v1.pdf>
- [16] T. Sjöstrand et al. *An Introduction to PYTHIA 8.2*. October 2014. url: <http://home.thep.lu.se/~torbjorn/pdfdoc/pythia8200.pdf>
- [17] ROOT. url: <https://root.cern.ch/>, accessed 15/12-2016

- [18] Script to plot the data and obtain the fit: <https://gitlab.cern.ch/atlas-phys-exotics-dmSummaryPlots/DMMassMediatorMass/blob/master/CompareSignalTemplates/allOffshellaxial-2.py>
Script to overlay two samples: <https://gitlab.cern.ch/atlas-phys-exotics-dmSummaryPlots/DMMassMediatorMass/blob/master/CompareSignalTemplates/SIOffANLO.py>
- [19] ATLAS Collaboration *Search for new phenomena in dijet mass and angular distributions from pp collisions at $\sqrt{s} = 13$ TeV with the ATLAS detector* March 2016. arXiv: <https://arxiv.org/pdf/1512.01530v5.pdf>
- [20] T. Skwarnicki *A Study of The Radiative Cascade Transitions Between The Upsilon-Prime And Upsilon Resonances*. PhD Thesis, 1986. url: <http://inspirehep.net/record/230779/files/f31-86-02.pdf>
- [21] R. Vogt *What is the Real K Factor?* July 2002. arXiv: <https://arxiv.org/pdf/hep-ph/0207359v1.pdf>
- [22] CMS Collaboration *Probing dark matter with CMS*. CERN Courier, September 2016. url: <http://cerncourier.com/cws/article/cern/66165>, accessed 8/12-2016

Appendices

Appendix A

Crystal Ball Function

The crystal ball function is given in two different cases:

- If $(x - \bar{x})/\sigma < -\alpha$ then the fit function is determined as follows:

$$\text{term1} = \left(\frac{n}{|\alpha|}\right)^n$$

$$\text{term2} = \exp\left(-\frac{\alpha^2}{2}\right)$$

$$\text{term3} = \frac{n}{|\alpha|} - |\alpha| - \frac{(x - \bar{x})}{\sigma}$$

$$\text{term4} = \text{term3}^n = \left(\frac{n}{|\alpha|} - |\alpha| - \frac{(x - \bar{x})}{\sigma}\right)^n$$

$$y = \frac{A \cdot \text{term1} \cdot \text{term2}}{\text{term4}} = \frac{A \left(\frac{n}{|\alpha|}\right)^n \exp\left(-\frac{\alpha^2}{2}\right)}{\left(\frac{n}{|\alpha|} - |\alpha| - \frac{(x - \bar{x})}{\sigma}\right)^n}. \quad (\text{A.1})$$

- For $(x - \bar{x})/\sigma > -\alpha$ the function becomes

$$y = A \exp\left(-\frac{x - \bar{x}}{2\sigma^2}\right), \quad (\text{A.2})$$

where A is the amplitude of the peak, \bar{x} , n , σ and α are parameters [20].

Appendix B

Fits

In this section, figures of the m_{jj} distribution including the fit are given for all cases that have not been displayed previously.

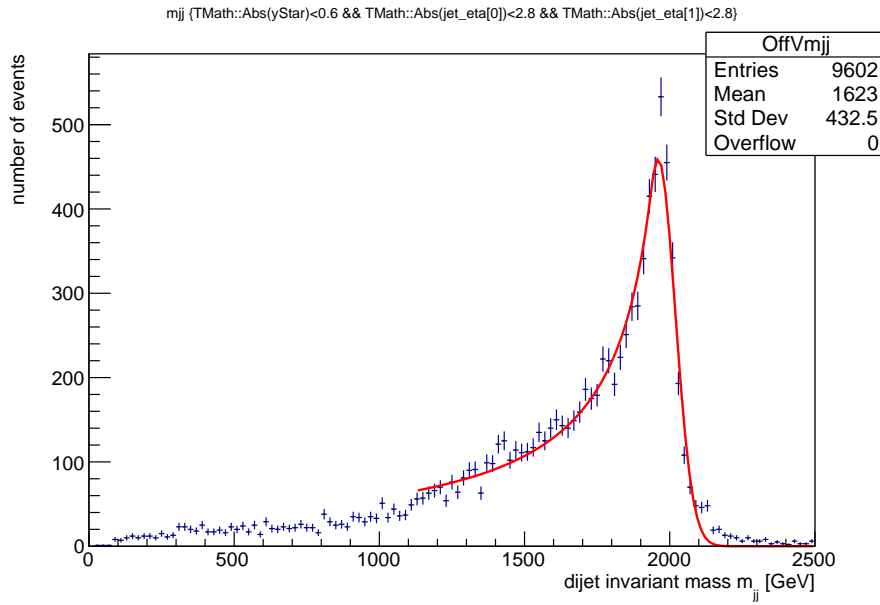


Figure B.1: Fit of the m_{jj} distribution for the off-shell, vector coupling sample

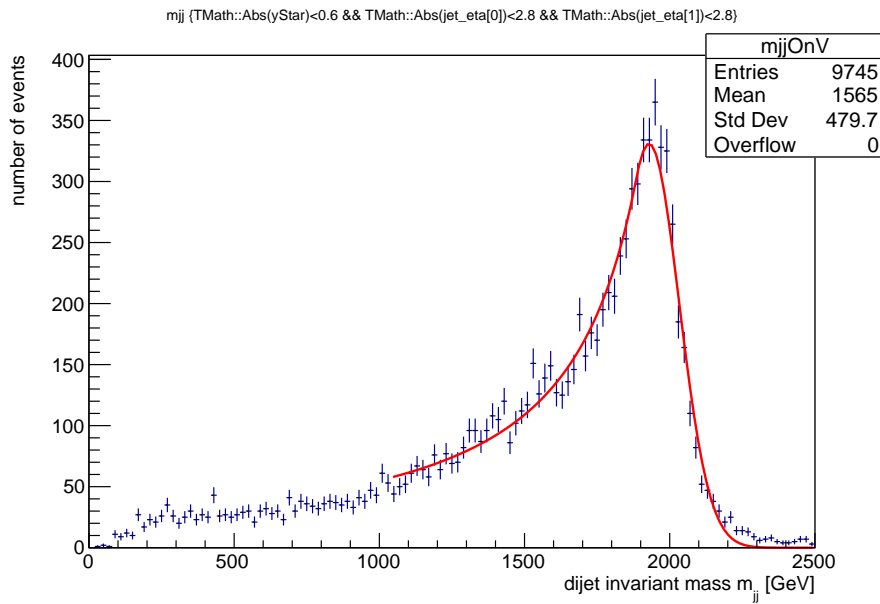


Figure B.2: Fit of the m_{jj} distribution for the on-shell, vector coupling sample

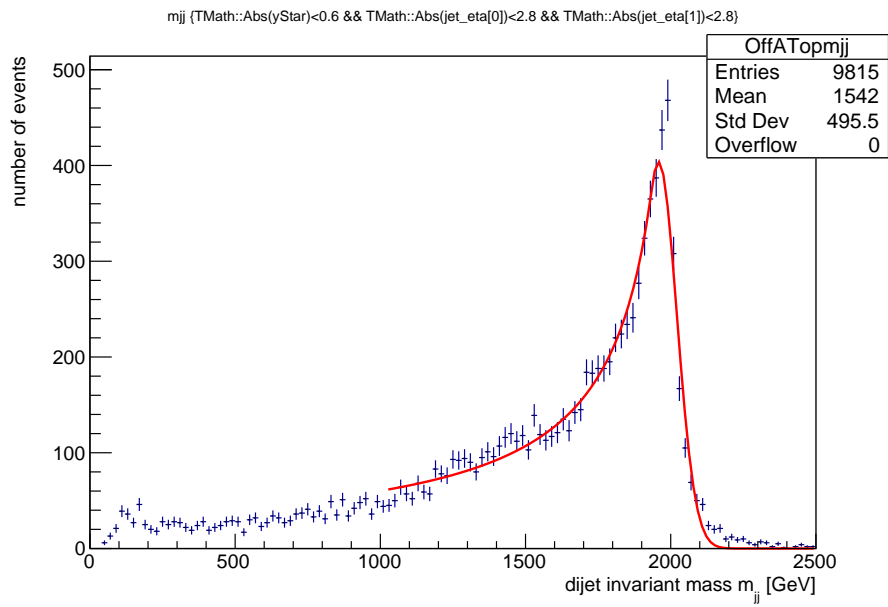


Figure B.3: Fit of the m_{jj} distribution for the off-shell, axial coupling including the top quark sample

Appendix C

Superimpositions

This section presents plots of m_{jj} , p_T , η and y^* for all samples overlaid with the nominal sample or other samples for comparison.

On-shell, axial sample:

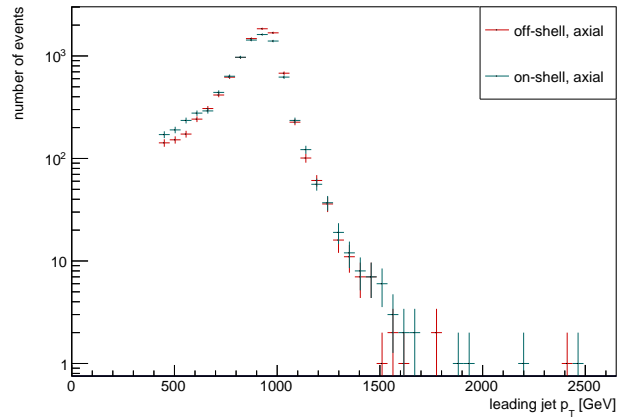


Figure C.1: Superimposition of the p_T with the on-shell axial sample

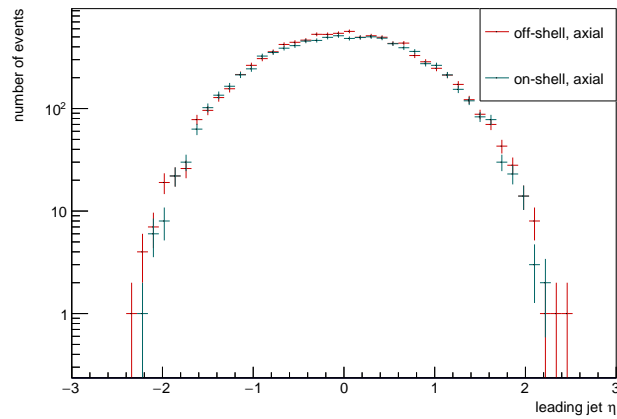


Figure C.2: Superimposition of the η with the sample with the on-shell axial sample

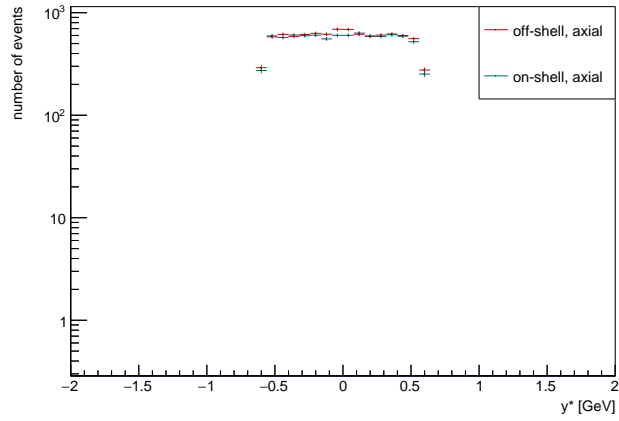


Figure C.3: Superimposition of the y^* with the on-shell axial sample

Off-shell, vector sample:

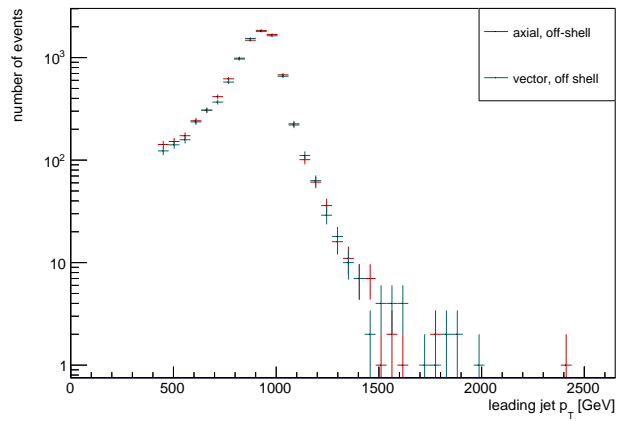


Figure C.4: Superimposition of the p_T with the off-shell vector sample

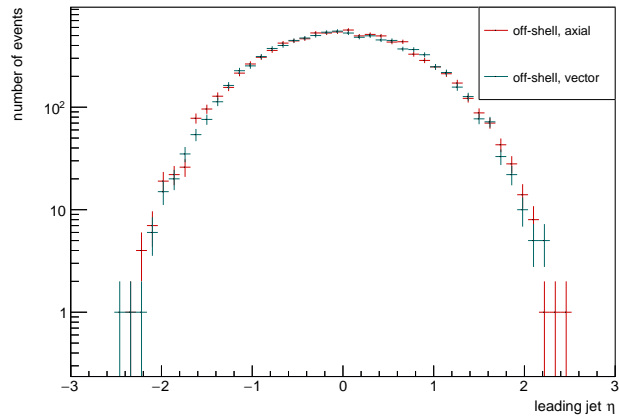


Figure C.5: Superimposition of the η with the off-shell vector sample

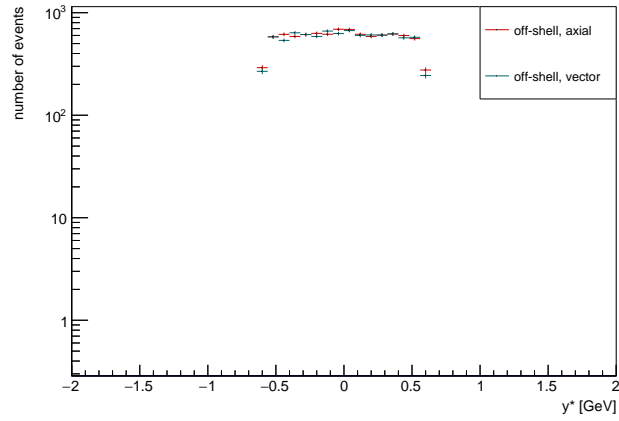


Figure C.6: Superimposition of the y^* with the off-shell vector sample

On-shell, vector sample:

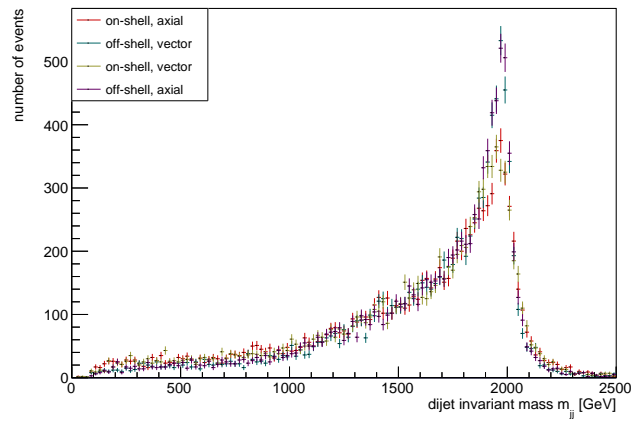


Figure C.7: Superimposition of the m_{jj} distribution with for all combinations of couplings with on- and off-shell

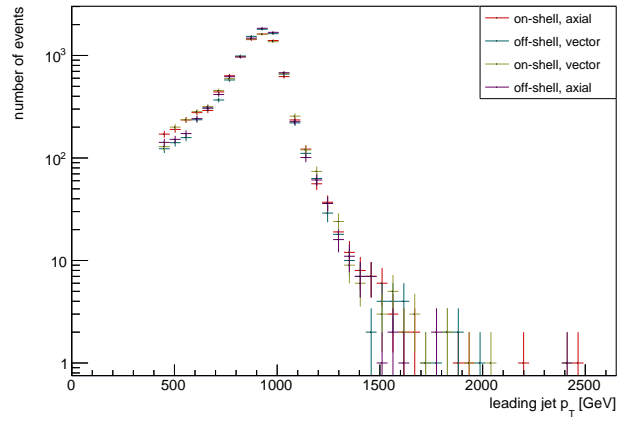


Figure C.8: Superimposition of the p_T distribution with for all combinations of couplings with on- and off-shell

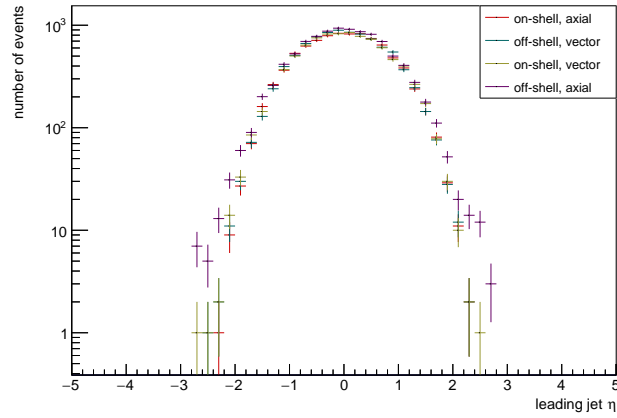


Figure C.9: Superimposition of the η distribution with for all combinations of couplings with on- and off-shell

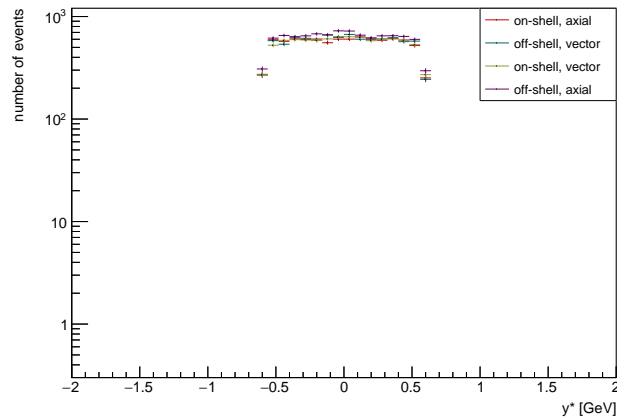


Figure C.10: Superimposition of the y^* distribution with for all combinations of couplings with on- and off-shell

Off-shell, axial with top quark sample:

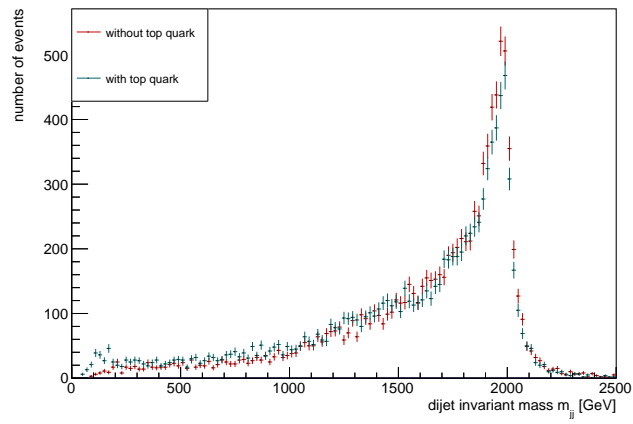


Figure C.11: Superimposition of the m_{jj} distributions with the sample including the top quark

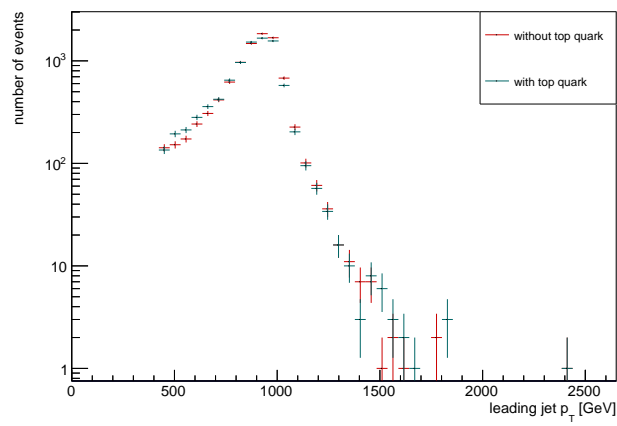


Figure C.12: Superimposition of the p_T distributions with the sample including the top quark

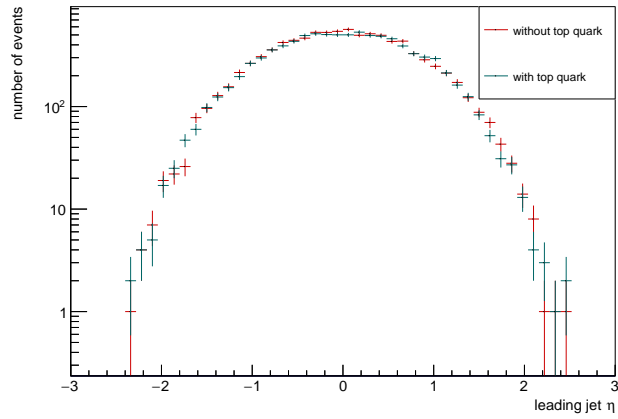


Figure C.13: Superimposition of the η distributions with the sample including the top quark

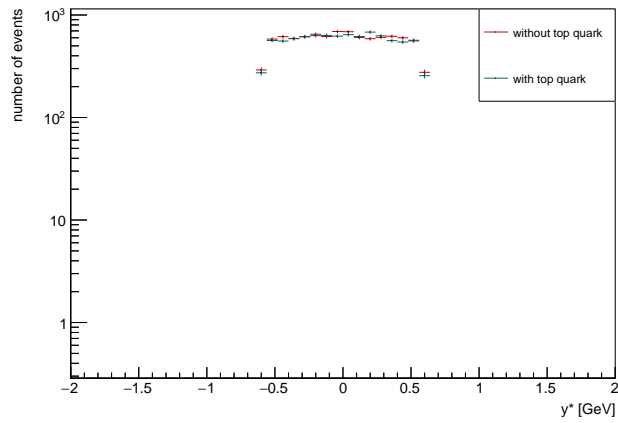


Figure C.14: Superimposition of the y^* distributions with the sample including the top quark

Off-shell, axial with NLO sample:

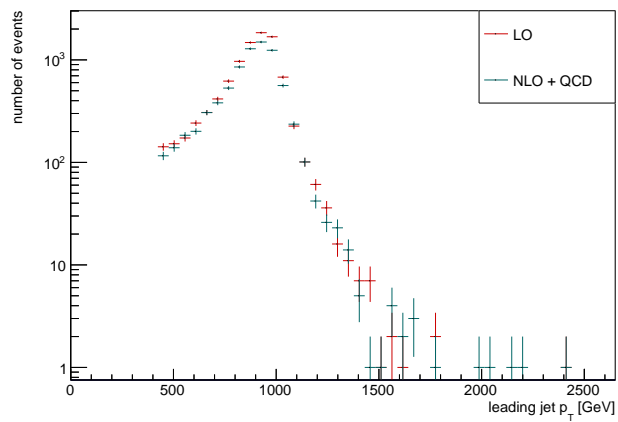


Figure C.15: Superimposition of the p_T distributions with the sample including NLO

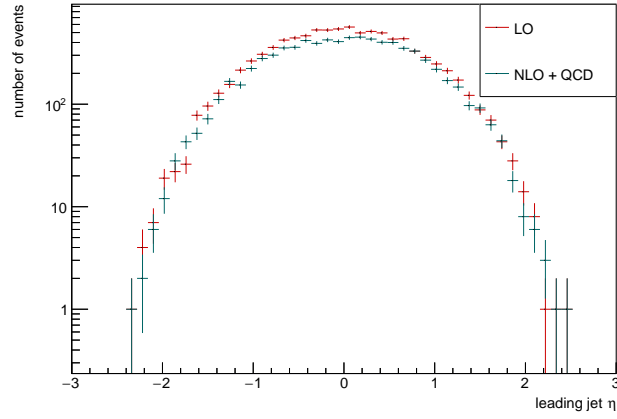


Figure C.16: Superimposition of the η distributions with the sample including NLO

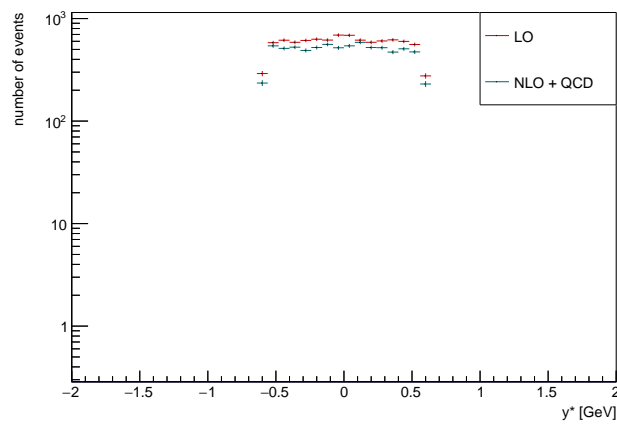


Figure C.17: Superimposition of the y^* distributions with the sample including NLO